https://doi.org/10.5194/egusphere-2024-3754
Preprint. Discussion started: 6 January 2025

Spatial error constraints reduce overfitting for potential field geophysical inversion

Mark Lindsay[1,2,3,4], Vitaliy Ogarko[3,4], Jeremie Giraud[4,5], Mosayeb Khademi[3,6]

[1] CSIRO Mineral Resources, Kensington, 6151, WA, Australia

[2] ARC ITTC Data Analytics for Resources and Environment, Perth, Australia

[3] MinEx CRC, Kensington, 6151, WA, Australia

[4] School of Earth Sciences, The University of Western Australia, Crawley, 6009, WA, Australia

[5] Laboratoire Géoressources, Université de Lorraine, Vandoeuvre-l`es-Nancy, France

[6] University of South Australia, Adelaide, 5000, SA, Australia

Correspondence to: Mark Lindsay (mark.lindsay@csiro.au)

Abstract: Geophysical inversion is an important tool for characterising the structure of the Earth. The utility of geophysical inversion has led to widespread adoption by resource explorers, and used to adapt gravity, magnetic, seismic and electrical datasets into petrophysical models that can be used for targeting. However, inherent ambiguity means that an infinite number of petrophysical models exist that can explain the geophysical data, so constraints such as geological models and petrophysical data have been employed to reduce the solution space. The constraints, like the data, are subject to noise and error resulting in uncertainty propagating to the final model. This is because inversion is designed to use the algorithm and constraints to find the 'best' solution by optimising the lowest misfit between the data and model. If the data is uncertain, the model fit to that data is likewise uncertain, and misrepresentative. Optimising misfit also means that inversion is subject to overfitting. Overfitting is when the lowest misfit values are attained by fitting the model to data noise. Overfitting inversion can create anomalies in the near-surface that can be mistakenly identified as legitimate targets for exploration rather than possible model artefacts. This contribution describes the use of spatial error constraints calculated from geophysical data to reduce overfitting for geophysical inversion. The spatial error estimate is derived from a geostatistical model calculated using Integrated Nested Laplacian Approximation (INLA). A region in the East Kimberley, northern Western Australia, is subject to gravity inversion using Tomofast-x, an open-source inversion platform. Inversion using different percentiles from the geophysical model explores whether the extrema of gravimetry values should be considered to explore the model space. Examination of inversion using and not using spatial error constraints shows that overfitting reduction can be achieved while using different percentiles as the observed field has lesser benefits.

1. Introduction

In geoscientific data, uncertainty can arise from various sources, impacting the accuracy and reliability of information. There are four broad categories of uncertainty that arise from scientifically-informed decision making: 1) incomplete scientific knowledge (i.e. epistemic uncertainty); 2) inherent variance

https://doi.org/10.5194/egusphere-2024-3754
Preprint. Discussion started: 6 January 2025

within the processes or systems under study making them difficult to measure consistently (i.e. aleatory uncertainty); 3) ambiguity and vagueness in communications between practitioners or organisations (i.e. linguistic uncertainty) and 4) how decisions are made in light of differing value for certain goals, objectives and trade-offs (i.e. value uncertainties) (Jessell et al. 2018; Quigley et al. 2019a). While all four categories are important when modelling the Earth, we focus on the aleatory and epistemic uncertainties.

Models using geoscientific data are thus subject to these uncertainties, either from the data (e.g. drilling data; Pakyuz-Charrier et al. 2018; geophysical data: Rashidifard et al. 2021; petrophysical data: Giraud et al. 2017; geochemistry: Johnson et al. 2024; structural data: Allmendinger et al. 2017) and assumptions that are used to build them (e.g. geological relationships: Brisson et al. 2023; interpolation parameters: Stoch et al. 2024) or from the manner in which they are interpreted (e.g. expert knowledge and bias: Torvela & Bond 2011; Wilson et al. 2019, geophysical modelling: Reid & Thurston 2014, human attention and observation patterns: Sivarajah et al. 2014) and used for decision-making (Quigley et al. 2019b). Recent efforts to understand the effects of these uncertainties have naturally led to producing model ensembles from perturbation of inputs and subsequent model construction to simulate the effects of data uncertainties (e.g. Caumon 2010; Lindsay et al. 2013; Murray et al 2016). A Bayesian inference framework is also well-suited to geoscience modelling problems, with the use of prior knowledge used to account for uncertainties in both data and model parameters and the data used as a likelihood (e.g. De La Varga et al. 2019; Olierook et al. 2021). Applications to both three-dimensional modelling and geophysical inversion have several robust and credible examples that focus on uncertainties in structural geological and petrophysical data (e.g. Giraud et al. 2019; Linde et al. 2017; Pakyuz-Charrier et al. 2018). Wellmann and Caumon (2018) provide a comprehensive review of such challenges in 3D modelling, and while not directly addressing the impacts on geophysical modelling, emphasise the considerable potential for compounding uncertainty in geophysical inversion given 3D geological models are routinely used as constraints (Guillen et al. 2008; Li & Oldenburg 1997).

Geophysical inversion is a commonly used technique in mineral exploration and near-mine studies that provide a realisation of continuous sub-surface properties that are impossible to obtain via rare drill core or outcrop observation. Geophysical inversion uses geophysical data as an observed field which the misfit between a proposed petrophysical model is measured. The most commonly used inversion approaches follow a deterministic approach, which, starting from a given model, will iterate through many solutions attempting to reduce the misfit using a cost function such as Tikhonov regularisation (a form of least squares or L2 Norm, Tikhonov & Arsenin, 1978). The inversion completes once the misfit between the petrophysical model and the observed field is below an acceptable threshold. A 'failed' inversion is when the threshold is not reached and converge to a geophysically satisfactory solution is not attained. The subsurface properties recovered from geophysical inversion are petrophysical in nature, which emphasises the need for petrophysical constraints, which variation is related to a range of geological properties (such as mineralogy, grain characteristics and texture, Dentith et al. 2020) emphasising the need for geological constraints to aid in solving an otherwise ill-posed and ambiguous problem with an infinite number solutions constituting the model space (Tarantola 2006). It is necessary to account for the uncertainty in the geophysical data used in the inversion to reduce the search space

https://doi.org/10.5194/egusphere-2024-3754
Preprint. Discussion started: 6 January 2025

and identify robust solutions belonging to the subset of the model corresponding to the available data (Tarantola, 2005).

Prior to introducing the proposed methods in more detail, it is useful to define some terms commonly used in this work: error, uncertainty and noise. Error is a specific deviation of the measured value away from the true value. Error is expressed as a single value, for example, when calculating the elevation of a gravity station, an error of -2 metres on a measurement of 248 metres would indicate the station is two metres lower that the true elevation of 250 metres. Uncertainty is a related yet broader concept describing the range and likelihood of errors, typically described as a distribution or range within which the true value is likely to fall. Measuring elevation may have a precision of ±5 metres, indicating the true elevation is between 245-255 metres. Noise refers to random processes that vary and distort the true value of a measurement. Noise can be attributed to instrument limitations, environmental factors, and other external factors that lead to measurement difficulties. For elevation measurements using GPS, noise can be attributed to antenna placement and quality, obstructions surrounding the location, or poor satellite positioning. For geophysics, noise can be related to environmental effects, such as weather or near-surface geology that is not otherwise accounted for when processing data during quality assurance and control.

1.1 Uncertain data for Geophysical Inversion

Geoscientific studies address uncertain data by: 1) truncation; 2) learning from it and; 3) using it as a modelling constraint. Truncation is simply identifying outliers and anomalous values and removing 'troublesome' data that imparts a bias to models sensitive to outliers (e.g. linear regression, principal component analysis, decision trees). Outliers may be attributed to analytical artefacts and poor sampling by conservative workflows supporting high-consequence decisions (resource evaluation, climate modelling). Learning from uncertain data takes a different view (Wellmann & Regenauer-Lieb, 2011), with the assumption that outliers or unexpected trends in data reveal latent patterns that can be attributed to some natural phenomena (e.g. presence of a subtle geophysical anomaly, or variations attributable to alteration) not explicitly recorded in the data. Such an approach is adopted by authors visualising uncertainty (references above) advocating for model uncertainty as knowledge. Thus, uncertainty can be used as an optimisation function for data collection (Pirot et al. 2019; Stamm et al. 2019) or using misfit in geophysical modelling to reveal geological objects not otherwise included in initial modelling efforts (Giraud et al. 2019; Lindsay et al. 2020).

Data uncertainty can be estimated using the covariance matrix of data errors (Scales & Snieder, 1998. A covariance matrix is a square matrix summarising the degree to which two random variables change (vary) together. Such uncertainties are typically attributed to data noise. However, Gouveia & Scales (1998) also include the (in)ability of a forward model to explain the data as a form of data uncertainty. Using a covariance matrix has been employed during seismic geophysical studies, where measurements are particularly susceptible to external noise sources (ambient sources such as wind, ocean waves, weather or cultural from nearby human activity) or when datasets are merged due to a dearth of measurements (Bodin et al. 2012). Noise can be unintentionally added if the merged datasets are from

https://doi.org/10.5194/egusphere-2024-3754
Preprint. Discussion started: 6 January 2025

different providers using different equipment ('batch effects'), or from different vintages, where the sensors themselves have different engineering specs and noise tolerances.

Noise is part of the data the model cannot explain and affects the size, shape and uncertainty of the non-uniqueness and ambiguity of the geophysical problem (known as the 'null-space' (Scales & Snieder, 1998). Thus, the covariance matrix provides a view of how measurements in a data set vary with every other measurement. High variability indicates measurements likely to contain more noise and low variability indicates measurements that form a pattern that describes the signal, and then used to remove noise. Chasseriau and Chouteau (2003) and Alsi et al (2000) address the noise problem of a forward model explaining the data using a geostatistical approach. Following Deutch and Journel (1992) and David (1997), Chasseriau and Chouteau (2003) use directional experimental variograms with sill and nugget values calculated from surface and drillhole density observations to condition the 3D density model for gravity inversion. The authors conduct a field example from the Blake River Group in the Abitibi Region, Canada and assume a data variance value of 0.1 $mGal^2$ for the gravity data, while also determining the directional experimental variograms to correct for regional effects. The inversion resolves various important geological features from the density model including geological bodies (the Flavarian pluton) and structure (Porcupine-Destor fault). Root-mean-square error (RMSE) from the model calculated with inversion is reported as 'infinitesimal' without density constraints, while 2.3% with constraints. While not explicitly stating so, the authors likely allude to an overfit and, thus, unrealistic density model if root-mean-squared-error (RMSE) values are suspiciously low. Overfitting is well-known and typical for unconstrained inversion of potential field data when the constraints are inadequate or do not suffice to prevent inversion from producing unrealistic, small-scale features fitting the data below noise or error levels. For gravity data, this may be due, in part, to the modelled gravity response decaying with the inverse-squared depth, which can be countered with depth weighting (Chasseriau & Chouteau, 2003) and a geological model with assigned petrophysical properties (e.g. Guillen at al. 2008). Overfitting may also be due to improper data weighting when, e.g., the data weighting scheme does not accurately reflect the relative reliability of different data points, which can lead inversion to fit some measurements too closely.

The geostatistical approach to geophysical inversion taken by Asli et al. (2000) and Chasseriau and Chouteau (2003) addresses the lack of resolution at depth for gravity inversion while increasing noise sensitivity and precision by cokriging density and gravimetric measurements to understand their covariance. The gravimetric/gravimetric and gravimetric/petrophysical covariances are not stationary, thus Asli et al. 2000 adopt a 'V-V' plot, a variographic version of the standard Q-Q plot. The theoretic covariance values between the gravity and density pairs and gravity and gravity pairs are arranged by increasing order and grouped from which a mean value is calculated. The grouping process relies on a semi-automated minimisation of the dispersion between the experimental gravity variogram, and theoretical variogram.

Shamsipour et al. 2010 take a similar geostatistical approach to gravity inversion using conditional simulation to identify the stable features of the inverted fields. This extends the work of Asli et al. 2000 to include uncertainty assessment. They found that conditional simulation allowed the parametrisation

https://doi.org/10.5194/egusphere-2024-3754
Preprint. Discussion started: 6 January 2025

of an exploration target by defining a maximum density gradient value while cokriging did not. The approach of Shamsipour et al. 2010 relies on the translation of mineral exploration criteria into petrophysical contrast value and could be helpful when searching for steep gradients, possibly associated with geologic structure (Clark & Schmidt, 2001; Dentith et al., 1994). Similar to Asli et al 2000, Shamsipour et al 2010 focus on the covariance of gravity data to density parameters, and modelled gravity, with data errors relating to gravity measurements.

1.2 Data inputs for inversion

The observed field for inversion is sourced from the measurements taken by the geophysical survey equipment. These may be recorded by gravimeters, magnetometers or various electromagnetic sensors. Corrections are required for geophysical data to account for known yet unwanted effects, such as ellipsoidal corrections for gravity data to account for the oblate shape of the Earth, and Bouguer correction to account for the elevation of the point above sea-level, the mass of that rock and for irregular terrain changes. The corrections are performed to isolate the geophysical anomalies caused by geological structures from those caused by surface topography. A quality assurance step should follow that examines the corrected observations to identify outliers or otherwise anomalous values, which then requires a decision to either remove outliers or keep them under the assumption they are representative of nature.

The corrected geophysical measurements are provided to the inversion as points or grids, with grids the format typically used. Grids are created through interpolation of the survey measurement to a regular mesh, which cell size typically serves the purposes of the modelling exercise. The chosen cell size is made considering the geometry of the geological objects one expects to resolve, topographic relief, and computational constraints (smaller cells and/or a larger model volume means more cells and will incur greater computational cost). The type of interpolation method includes geostatistical methods like kriging, Bayesian models and radial basis functions and deterministic methods like inverse distance weighting and splines (Myers 1994). Geostatistical methods evaluate spatial structure and dependence using a variogram or covariance matrix, provide uncertainty quantification, and offer many constraints to control the process. Deterministic methods are simpler, requiring little (if any) constraints and can handle higher data volumes, however do not offer uncertainty quantification or a statistical model for spatial structure and dependence. Geoscientists have traditionally used deterministic interpolation methods, however increased computing power, approximation methods for geostatistical interpolators combined with more intuitive constraint assignment and the needs for uncertainty quantification of large datasets mean that geostatistical methods being readily adopted for spatial analyses (Cressie et al. 2022; Sainsbury-Dale et al. 2024).

A covariance matrix, populated with measurement errors, including geostatistical error estimates can help support the use of points or interpolated grids. This is important to include, otherwise the inversion will assume: 1) the measurements contain no error and; 2) the interpolation always predicts true values, even those at some distance from measurements and affected with ‘spatial error’. These assumptions are false. While geophysical data collection is undertaken with much care and attention to minimising noise and error via precision engineering or reducing environmental effects (Fairhead et al. 2017; Boddice et

https://doi.org/10.5194/egusphere-2024-3754
Preprint. Discussion started: 6 January 2025

al. 2018, Lane et al. 2019), it is unrealistic to expect all sources of noise and error can be accounted for. Likewise, it is unrealistic to expect interpolation to perfectly reproduce the true values of a natural process from noisy, sparse and clustered data typical of the geosciences (Karpatne et al. 2019).

Conditioning inversion with measurement error is used in geophysics (e.g. Asli et al. 2000, Shamsipour et al. 2010; Bodin et al. 2012). This contribution considers the uncertainty inherent when using interpolated grids as the observed field and the effect on inversion. We hypothesise that a covariance matrix populated with geostatistical error estimates, or 'spatial error' (as used for the rest of this manuscript) associated with interpolation can support inversion by facilitating targeted misfit reduction in uncertain locations and reducing overfitting.

The benefit of targeting uncertain locations prone to data noise and error is that the inversion can be optimised to focus parameter changes in these regions to find a low misfit petrophysical solution, and to restrict the inversion search space to models adequately fitting the data. The weighting can be applied in two ways. One is to allow lower misfit thresholds given the observed field is now understood to be less likely close to the true value in uncertain regions. Allowing lower thresholds for regions supported by uncertain data will also help to avoid overfitting. The second approach is to focus parameter changes in parts of the petrophysical model which are supported by uncertain regions interpolated grid. The rationale is that more parameter combinations will also be plausible with greater uncertainty in those regions.

The contribution described below is reminiscent of a Bayesian framework, where the likelihood (the probability of observing the data given specific parameter values) usually includes an error term (Gelman et al. 2013). Likewise, we explore different 'slices' of the posterior distribution of estimated gravity values, subjecting them to inversion and comparing the results. A fully-developed Bayesian approach to inversion can achieve similar aims (e.g. magnetotellurics: Seille et al. 2021; and seismology: Sambridge et al. 2013). The approach we demonstrate is not as sophisticated as those cited above, however does avoid controversy around selection of a prior distribution within a strictly Bayesian framework (Scales & Snieder, 1997; McGrayne, 2011). Thus, we demonstrate a workflow typical of those used by exploration geophysics practitioners where a grid interpolated from a set of gravity measurements us used as the observed field to calculate misfit between the field calculated from the proposed geological model (e.g. Fullagar et al. 2000; Lelièvre et al. 2009). The interpolation is typically executed using a bicubic, nearest neighbour or spline algorithm, thus deterministic and offering a single grid representation which ignores the possibility of alternative grid models. While these alternative models are less likely, they are nonetheless plausible given noisy and error prone measurements taken of natural phenomena. We explore the extrema of these alternatives with geophysical inversion and evaluate the value of uncertainty estimates as a critical constraint.

1.3 Study area

The eastern part of the Kimberley region is examined in the area around the Savanna Ni-Cu-Co mine (Figure 1). The terrane hosting the Savanna mine is the Halls Creek Orogen, which is separated into the western, central and eastern zones based on differing tectonostratigraphic characteristics (Tyler et al., 1995). The siliciclastic Kimberley Basin and mafic rocks of the Hart-Carson Large Igneous Province (LIP) bound the western edge of the Halls Creek Orogen. The western zone of the Halls Creek Orogen

https://doi.org/10.5194/egusphere-2024-3754
Preprint. Discussion started: 6 January 2025

is characterised by the felsic to mafic rocks of the Paperbark Supersuite, Whitewater Volcanics and Ruins Dolerite, with the mafic and felsic rocks thought deposited contemporaneously around 1859 to 1853 Ma (Blake et al. 2000; Page and Hoatson, 2000). The central zone is characterised by amphibolite to granulite facies Tickalara Metamorphics and mafic to ultramafic Savanna, Panton and Sally Mally intrusions. Later intrusion of voluminous felsic to mafic magmas between 1837 and 1808 Ma formed the Sally Downs Supersuite (Tyler & Phillips, 2021) and the most common outcropping rocks in the central zone. The eastern zone is characterised by siliciclastic and volcanic rocks. The eastern edge of the Halls Creek Orogen is bounded by the sedimentary and volcanic rocks of the Ord Basin, sedimentary rocks of the Wolfe Basin, and mafic to ultramafic rocks of the Kalkarindji LIP. Three structures, either shear zone or major faults, trending south-southwest and north-northeast are interpreted to intersect the region. Large density contrasts between the sedimentary or felsic rocks and mafic and ultramafic rocks (Lindsay et al. 2016), which are represented in the gravity data (Figure 2) make this region an appropriate location for using gravity data for inversion. Likewise, previous forward modelling and petrophysically-constrained geological interpretation by Lindsay et al. 2016 suggests the strong and positive gravity anomalies are consistent with a combination of near-surface mafic intrusions and an interpreted deeper, voluminous mafic body. The forward modelling of Lindsay et al. 2016 is used as a plausibility check for inversion. While the forward model is by no means conclusive nor exhaustive, it was constructed using a different method independent from this work. The same data is incorporated and includes geological knowledge, thus we believe it an appropriate control for comparison.

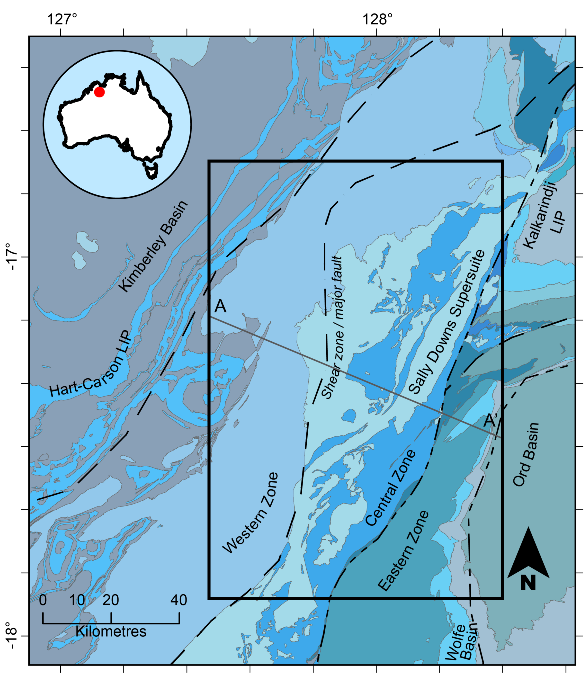

Figure 1. Geological map of the East Kimberley region, northern Western Australia. The major tectonostratigraphic terranes relevant to this study are labelled, with interpreted major shear zones and faults

https://doi.org/10.5194/egusphere-2024-3754
Preprint. Discussion started: 6 January 2025

labelled with italics and indicated with dashed lines (Geological Survey of Western Australia, 2022). The solid black box indicates the region of interest. The grey line marked A-A' indicates the position of the section shown in Figure 9. The inset map (top left) shows the position of the region of interest within Australia.

2. Methods

The demonstration of using geostatistical spatial error constraints with geophysical inversion requires four components: the dataset, a geostatistical method, an inversion framework and an evaluation procedure. Here, the dataset is gravity data supplied by Geoscience Australia (Sect 2.1), the geostatistical method is provided by the INLA (Integrated Nested Laplacian Approximation; Rue at al., 2009) package using R (Sect. 2.2), the inversion was conducted using the Tomofast-x inversion platform (Sect. 2.3) from which different statistical measures are used to evaluate the efficacy of the method.

2.1 Data

Gravity data is supplied by Geoscience Australia as geolocated points (Figure 2) (Geoscience Australia, 2020). Gravity station locations are spaced at 400 to 900 m on roads and around 11 km elsewhere. The relevant attributes used for gravity modelling are spatial coordinates in GDA94 (latitude and longitude in decimal degrees) and the spherical cap Bouguer anomaly (SCBA) corrected data (Lane et al. 2019). A subset of the national compilation were created using spatial coordinates that conform to the boundaries of the region of interest (Figure 1). Grids were interpolated to 1000 m (lower resolution) and 500 m (higher resolution) cell sizes.

2.2 Geostatistical modelling

Geostatistical modelling was undertaken using approximate Bayesian inference facilitated by the "INLA" package (Rue et al. 2009) for the "R" scientific computing language (R Core Team, 2023) in R Studio (Posit Team, 2023). INLA is a Bayesian inference method for latent Gaussian models designed to provide fast approximations of posterior distributions from complex models that may be computationally expensive or infeasible when using Markov Chain Monte Carlo (MCMC) methods. INLA is adapted for geostatistical analysis due to rapid computation and acceptable accuracy for most natural science questions (Cressie et al. 2022; Morgana, 2023; Wang & Zuo, 2021). INLA provides many of the same metrics required of geostatistical analysis for this study (accuracy and uncertainty estimates) while being able to interpolate large datasets faster than most other geostatistical packages (Cressie et al. 2022). While the data set we use in this study ($n = 707$) is not large, using INLA in the workflow allows easy adaption to studies requiring large data sets (e.g. $n > 1M$). To our knowledge, this is the first time outputs from INLA are used as inputs for potential field geophysical inversion.

INLA derives the standard deviation of the predicted quantity, in this case, gravitational acceleration, from the estimated posterior distribution. First, a Laplace approximation integrates out the latent variables from the model. The Laplacian approximation produces a Gaussian approximation of the posterior distribution for the parameters of interest. INLA estimates the mean, any quantile and standard deviation from the marginal distribution for each parameter (Rue et al. 2009; Morgana, 2019, 2023). The standard deviation is used to construct the spatial error grid. The mean of the marginal distribution is

https://doi.org/10.5194/egusphere-2024-3754
Preprint. Discussion started: 6 January 2025

used to construct the 'mean' grid and can be considered equivalent to interpolated grids typically used as observed fields for inversion. The 2.5th and 97.5th quantiles from the marginal distribution are used to construct the lower limit ('ll') and upper limit ('ul') grids, respectively.

2.3 Geophysical inversion

Tomofast-x is an open-source geophysical inversion package designed for gravity and magnetic data and used for mineral exploration and crustal studies (Giraud et al. 2021; Ogarko et al. 2024). Tomofast-x 2.0 offers parallel computing and wavelet compression of the sensitivity matrix, which aid the computational requirements of the inversion while providing several useful performance metrics used in assessing the convergence and inversion results. These include the data misfit and the evolution of the different constraint terms during the inversion. In particular, the petrophysical-bounding constraints term is used, which is enforced by the ADMM technique (alternating direction method of multipliers, a statistical petrophysical constraint, see Ogarko et al. 2021). Another metric includes the cross-gradient value, used and applied to each cell when using structural constraints (using an extension of Gallardo et al. 2003), and the likelihood of (or a mixture of) a petrophysical distribution characterising a particular lithology.

The objective function to be minimized includes the following data misfit term:

$$\Phi_d = \|\boldsymbol{W}_d(\boldsymbol{d}^{calc} - \boldsymbol{d}^{obs})\|_2^2, \quad (1)$$

where $\boldsymbol{d}^{calc}$ and $\boldsymbol{d}^{obs}$ represent the calculated and observed (field) data, respectively. $\boldsymbol{W}_d$ is a diagonal weighting matrix with the i-th element equal to $1/\sigma_i$, where σ_i denotes the standard deviation of the i-th datum (Li & Oldenburg, 1996). We use the INLA standard deviation (as described in Sec 2.2) for σ_i, representing the spatial data error introduced by data gridding. In the cases when data error is disregarded, we set $\boldsymbol{W}_d = \boldsymbol{I}$, with $\boldsymbol{I}$ being the identity matrix, thus weighting all data equally, irrespective of location.

The model domain used for inversion was constructed using 1000 m (lower resolution) and 500 m (higher resolution) cell sizes. The domain was given 10000 m of padding to mitigate boundary effects and enhance numerical stability (Zhdanov, 2002).

2.5 **Performance metrics**

Two performance metrics are used in evaluating the results of this research: the relative residual level (RRL) and data cost.

RRL: The relative residual level found by the LSQR solver (Paige and Saunders, 1982). The desired result is for the RRL to be high, meaning lower variance and thus lower uncertainty in the model prediction. The desired full-convergence is achieved when RRL values approach an upper bound of 1.0.

Data Cost: A dimensionless measure cost=$\|\boldsymbol{d}^{calc} - \boldsymbol{d}^{obs}\| / \|\boldsymbol{d}^{obs}\|$. The desired result is for lower values. Data cost is a normalised version of RMSE and better represents changes in misfit with each iteration as it is less sensitive to outlier values.

https://doi.org/10.5194/egusphere-2024-3754
Preprint. Discussion started: 6 January 2025

1. Results

We assess the results from inversion using RRL and data cost. Each of these metrics describe different aspects of inversion performance. Visualisation of the inputs and results for each inversion are then presented.

3.1 Inversion inputs

Inversion was conducted using different reference gravity field data sets:

1) data points represented gravity field observations as obtained from Geoscience Australia;
2) a grid interpolated from gravity field observations represented the mean estimated values a.k.a the 'mean model';
3) a grid interpolated from gravity field observations representing the 2.5th quantile, or lower limit of estimated values a.k.a. the 'lower limit model' and;
4) a grid interpolated from gravity field observations representing the 97.5th quantile of estimated values, a.k.a. the 'upper limit' model.

Each of the grids have a cell size of 1000 m based on the closer 400 m spacing of stations located close to roads. We use 500 m cell size for detailed analysis of the relationship between spatial error and misfit (Section 3.5).

Figure 3 displays the spatial and statistical distributions for the point measurement data and interpolated grids. The bi-modal shape of the point measurement distribution generally replicated in the interpolated grids. Smoothing effects in the histograms for the interpolated grids can be seen, especially in values $200 < x < 600$. The histogram shape of the interpolated values are quite similar with expected positive skew for the lower limit grid and negative skew (though not as obvious) for the upper limit grid when compared to the mean grid histogram. A north-northeast trending positive gravity anomaly located in the centre of the region of interest is the most obvious feature revealed by the spatially plotted data and grids. Smaller positive anomalies are located south and south-southwest of the main anomaly. Negative gravity anomalies are located in the northwest and southwest of the region, and are most obvious in the interpolated grids. The lower and upper limit grids reveal small circular anomalies which are collocated with the station observation locations. The circular anomalies exhibit higher gravitation values than the general trend in the lower limit grid, and lower values than the general trend in the upper limit grid. This effect is due to the interpolation honouring the observations, and being sampled from the tails of the geostatistical model. Thus these anomalies are not visible in the mean grid.

The mean grid represents an equivalent to the grid typically input to inversion as the observed field, such as minimum curvature or bi-cubic interpolation (Swain, 1976). A comparison between the mean grid and a minimum curvature grid interpolation reveals an RMSE = 9.78 μms^{-2} and σ = 9.46 μms^{-2} of the residual between the two grids. Small differences are expected given two different interpolators are used (INLA and minimum curvature). The RMSE of the residual is 0.8% of the total range of the mean grid. A small percentage shows these differences are small and inversion will not be biased to the chosen interpolator.

https://doi.org/10.5194/egusphere-2024-3754
Preprint. Discussion started: 6 January 2025

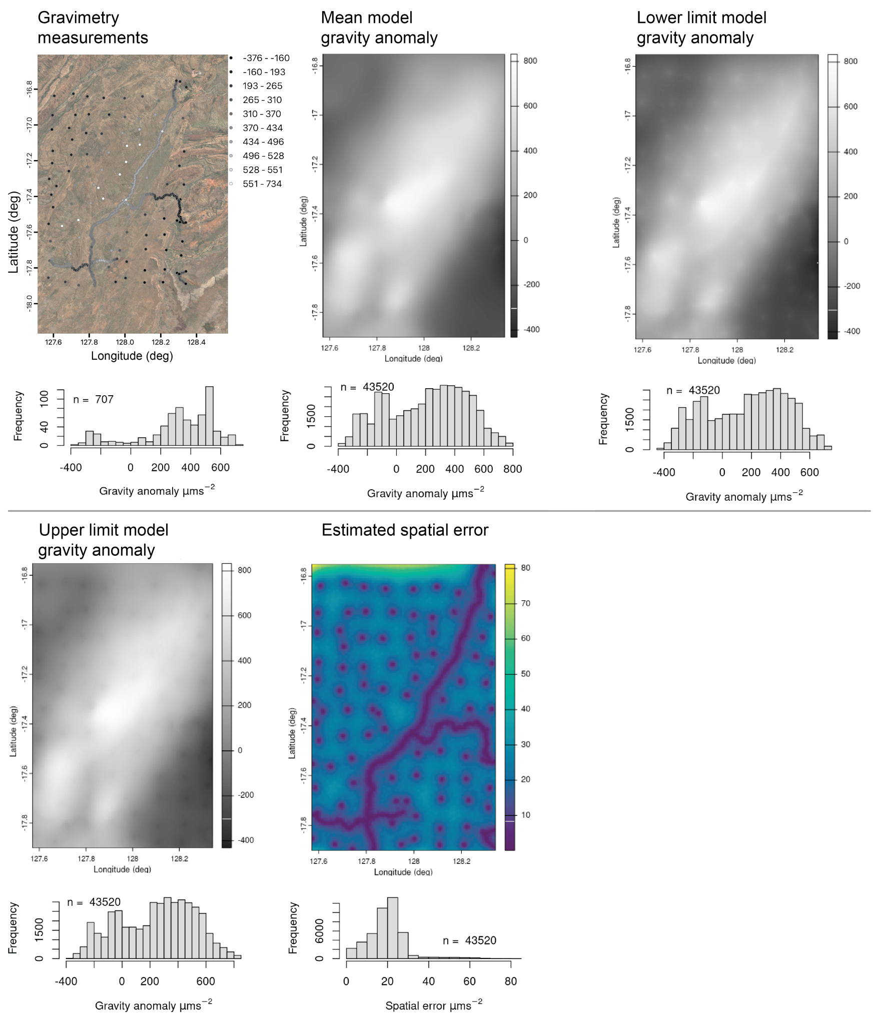

Figure 2. Spatial and statistical distributions of gravity point measurements and grids from the region of interest in the East Kimberley. (L-R) Shown are point observations, mean model, lower limit, upper limit and estimated spatial error. The histogram associated with each point set or grid is shown underneath. Satellite imagery © 2024 TerraMetrics.

3.2 Inversion iterations

The reduction in data cost from the initial model to the final inverted model determines the number of iterations required for inversion convergence. We use the 'mean model' for this purpose. A run of 10 iterations resulted in a reduction of 80% of the RMSE, a run of 20 iterations increased this to a reduction in 85% of RMSE and 30 iterations reduced RMSE to 86%. Twenty iterations are considered an appropriate by balancing some reduction in RMSE (10 versus 20 iterations), and avoiding potential overfitting with 30 iterations with little improvement in RMSE. The charts and visualisations in the following section are obtained from the model runs of 20 iterations.

https://doi.org/10.5194/egusphere-2024-3754
Preprint. Discussion started: 6 January 2025

3.3 Inversion results.

The results are presented in the following order. First, we present the performance metrics for models using: data points only; gridded gravity data; gridded gravity data and spatial error values input to populate the covariance function. Then visualisation comparing the inversion results for each of these model groups is presented.

Figure 3 displays results from inversion using point representation of the observed gravity field. The data cost decreases from 1.0 to 1.64 x 10^{-4}. RRL values increase from 7.82 x 10^{-4} to 0.98, indicating the solution has achieved full convergence.

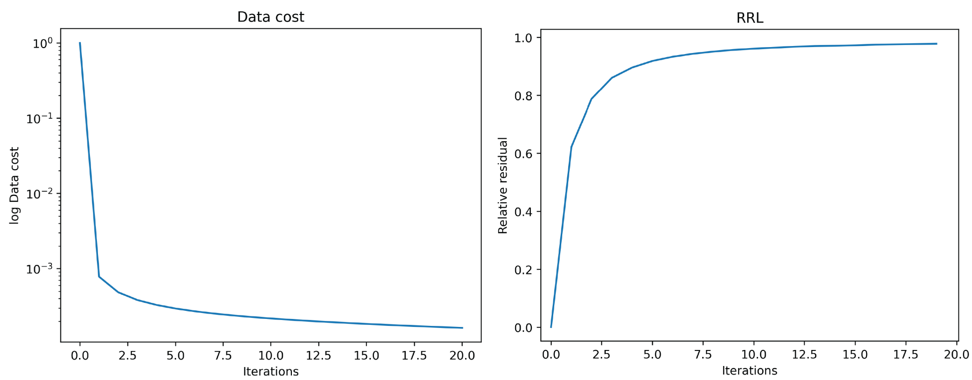

Figure 3. Data cost (left) and relative residual (right) results from inversion using point gravity measurements as the objective field.

Figure 4 compares performance metrics from inversion using gridded models as objective fields. Each of the mean, lower limit and upper limit models are shown. The top row displays metrics from inversion that did not use spatial error constraints. The bottom row displays metrics from inversion that did use spatial error constraints. The data cost results show the mean grid models produce lower misfit than the lower and upper limit models. There is no meaningful difference between the performance of the lower and upper limit models. The relative residual results are also similar between inversion using and not using spatial error constraints, with RRL values just under 1.0 indicating convergence being achieved.

https://doi.org/10.5194/egusphere-2024-3754
Preprint. Discussion started: 6 January 2025

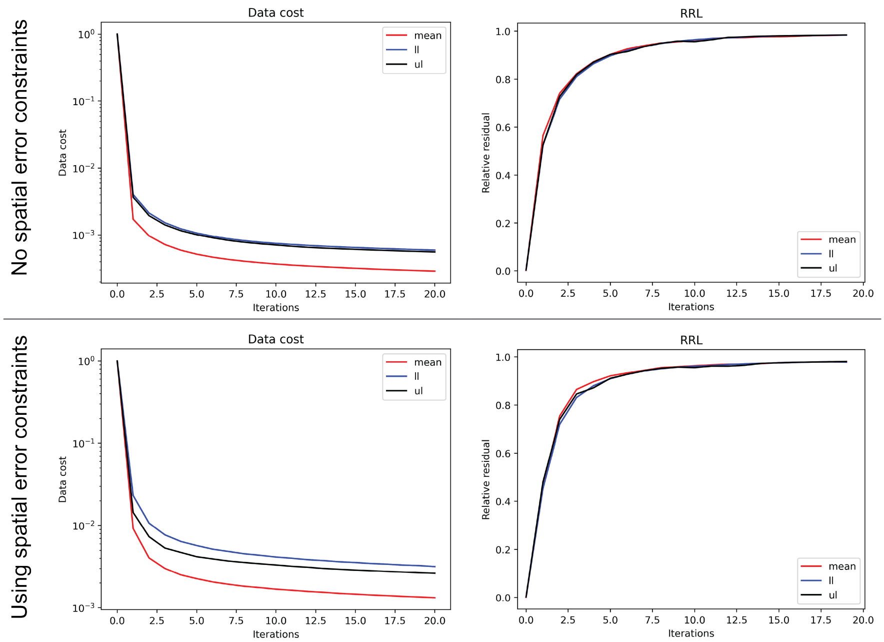

Figure 4. Comparison of data cost and relative residual performance metrics for each gravity model. Data cost is shown using a log scale. Models using not using spatial error constraints are on the top row, those using spatial error constraints are on the bottom row. 'll: lower limit; 'ul': upper limit.

Another comparison is shown in Figure 5. Here we compare all inversion results, including that using measurement points, for each performance metrics. Note the data cost is shown with a log scale. The lowest misfit is achieved from inversions not using spatial error constraints, with the lowest data cost values from inversion using measurement points (data cost at iteration 20 = 1.6 x 10^{-4}), followed by the mean gridded model with no spatial error constraints (data cost = 2.9 x 10^{-4}). The mean gridded model using spatial error constraints shows data cost = 1.3 x 10^{-3}) almost an order of magnitude higher.

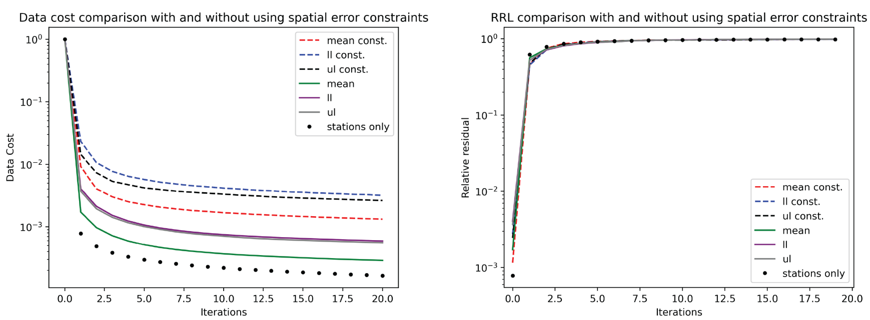

Figure 5. Comparison of performance metrics for different gridded and station measurement inputs using and not using a spatial error constraints. Left: Data cost; right: relative residual; 'll: lower limit; 'ul': upper limit. Note inversion using station measurements does not use spatial error constraints.

https://doi.org/10.5194/egusphere-2024-3754
Preprint. Discussion started: 6 January 2025

We can check whether the inversion has adequately reduced misfit over all iterations and all model inputs. Table 1 shows the reduction in RMSE misfit, a typical method used to evaluate the efficacy of an inversion (e.g. Farquharson & Oldenburg, 1998; Lindsay et al. 2014). All values are close to or > 80% indicating an adequate misfit reduction. Thus, we can be confident the inversion reduces misfit at a similar rate from one iteration to the other regardless of input and the use of a spatial error representation.

Table 1. Reduction of misfit for each inversion using different inputs. ll: lower limit; ul: upper limit, 'const.': constrained with spatial error. Reduction is calculated by subtracting the RMSE misfit of the initial iteration from the final iteration.

Input	Reduction in misfit
mean const.	85%
ll const.	87%
ul const.	86%
mean	83%
ll	85%
ul	85%
Stations only	79%

Misfit reductions produced by using a spatial error constraints are larger, but similar to the other results. The misfit reduction of inversion using the point measurements is the lowest, but still large and not markedly different. Thus, we next visually examine inversion results to evaluate: 1) whether they look sensible and; 2) whether they vary from each other.

3.4 Inversion Visualisation

Inversion results are shown with the low and high density anomalies to aid visualisation (Figure 6). Relative density is used, which is density values relative to background density of 2670 kg/m^3. The thresholds for the relative density values were chosen mainly to aid visualisation of interesting geobodies rather than by some sophisticated statistical measure. Note while the range of values for each inversion is different (Figure 6), the low threshold value for the high density values is constant for all model visualisations. Likewise for the high threshold value for the lowest density values.

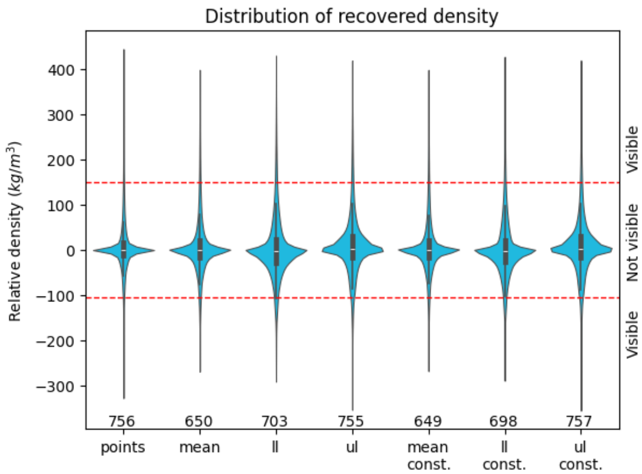

Figure 6. Distribution recovered density values from each inversion: ll: lower limit; ul: upper limit, 'const.': constrained with spatial error. The red horizontal lines indicate the low and high thresholds for highlighting the lowest and highest density anomalies. The numbers at the base of each column are the range of relative density values for each model in kgm^{-3}.

The range of values for each model reveals some patterns. The greatest ranges are seen with the inversions of observations and the upper limit data sets. The smallest ranges are associated with the interpolated datasets using mean values. Use of spatial error constraints does not appear to influence the range of values across these datasets, unlike the results of the data cost metric (Figures 4 & 5).

Figure 7 displays the results of inversion when using only the gravity observations at station locations as the observed field (Figure 2). Figure 8 displays results of inversions when interpolated grids are used as the observed field. Recall that not all voxels are shown as thresholds on the density values are used (Figure 6) to highlight certain interesting patterns from the visualisations.

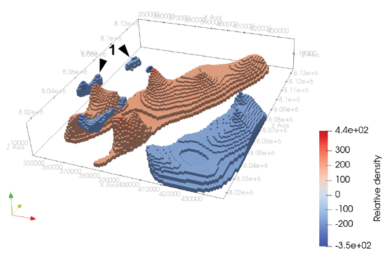

Figure 7. Relative density visualisation of inversion using point gravity measurements viewed from the southeast. Density values have been filtered according to the thresholds shown in Figure 6.

https://doi.org/10.5194/egusphere-2024-3754
Preprint. Discussion started: 6 January 2025

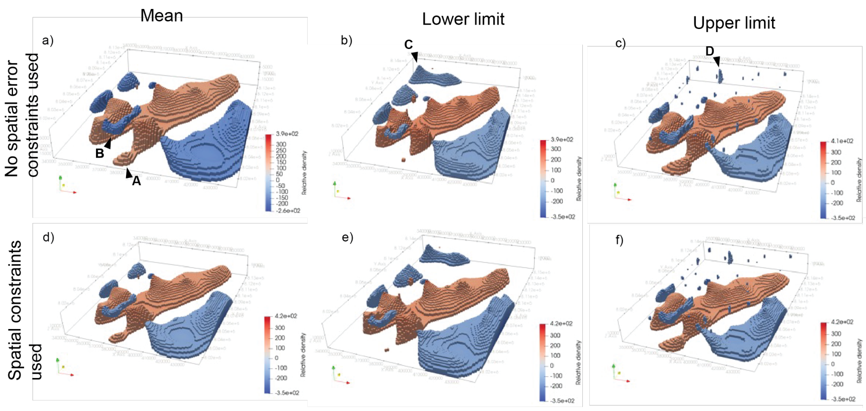

Figure 8. Relative density visualisations of inversion using gridded data viewed from the southeast. The top row are models not constrained by spatial error; the bottom row are models that have been constrained using spatial error. Density values have been filtered according to the thresholds shown in Figure 6.

Overall, the geometry of all inversions are similar, however the most obvious differences are seen between inversions performed using data points only, the mean, lower and upper limit models. Location 1 (Figure 7) shows low density bodies that exhibit smaller volumes as compared to the equivalent locations in Figure 8, in particular parts c) and f) (the upper limit models). Location A (Figure 8) is a northeast-trending low density anomaly that changes volume when compared to the lower limit models, but is similar to the upper limit models. Likewise, Location B is a high density body that would appear to change volume when compared to the lower limit models, but is similar to equivalent locations in the upper limit models. Location C in the lower limit models is a low density anomaly that is absent in the points, mean and upper limit models. Location D indicates not a single low density anomaly but an example of a number of small scattered low anomalies through the upper limit model that are absent in the mean and lower limit models. Of note are the lack of significant differences between equivalent models using and not using spatial error information (e.g. the mean interpolated values, a) and d). While minor differences can be seen (e.g. a slightly smaller high density anomaly at location A in the mean model using spatial error constraints - d)), they are not as obvious as those between the different observed field types.

Whether inversion results are geologically realistic, or simply plausible, is important to assess. Such realism and plausibility usually come in the form of independent constraints from a prior geological model (Gallardo et al. 2005), from petrophysical measurements (Fullagar et al. 2000) and sometimes both (Guillen et al. 2008). Thus, the infinite number of solutions an inversion can produce is then restricted to only those that are consistent with known geologic structure and petrophysical properties. The study presented here diverges from this practice and performs unconstrained inversion, i.e. inversion that does not use a prior geological model, nor petrophysical constraints. An unconstrained approach is admittedly not 'best practice' but nonetheless useful to clearly evaluate the effect of spatial error constraints on inversion without other constraints in use. So, assessment of inversion results and plausibility is achieved by comparing with previous work by Lindsay et al. (2016) who performed

https://doi.org/10.5194/egusphere-2024-3754
Preprint. Discussion started: 6 January 2025

forward geophysical modelling using petrophysical data collected from the region, and using both gravity and magnetic data (Figure 9).

Figure 9a shows the how the data is reproduced by the petrophysical model (part b). Part c) is a section taken from inversion of the mean model constrained with spatial error. Note the section c) is to 15 km depth, so an outline of the extent has been added to part b for easier comparison. The units of in each section are not the same (absolute density values in b versus relative in c), however we can colocated high and low values to assess plausibility. The broad positive density anomaly through the centre and bottom half of section b is observed in section c. The main difference is that anomaly in section c extends further into the shallow parts of the crust at ~ 4 km. There are shallower dense bodies modelled in b (at ~ 4km depth and distance = 60 km) that can account for this, and that the more extensive dense body in c could be separated if provided with an adequate structural prior model. Strong, low density regions at the edges of section b are also replicated in similar locations in section c. More geologically detailed bodies at the near surface in section b can be observed in section c with high frequency lateral changes in the density structure. The inversion results are plausible, especially given no geological and petrophysical constraints were provided.

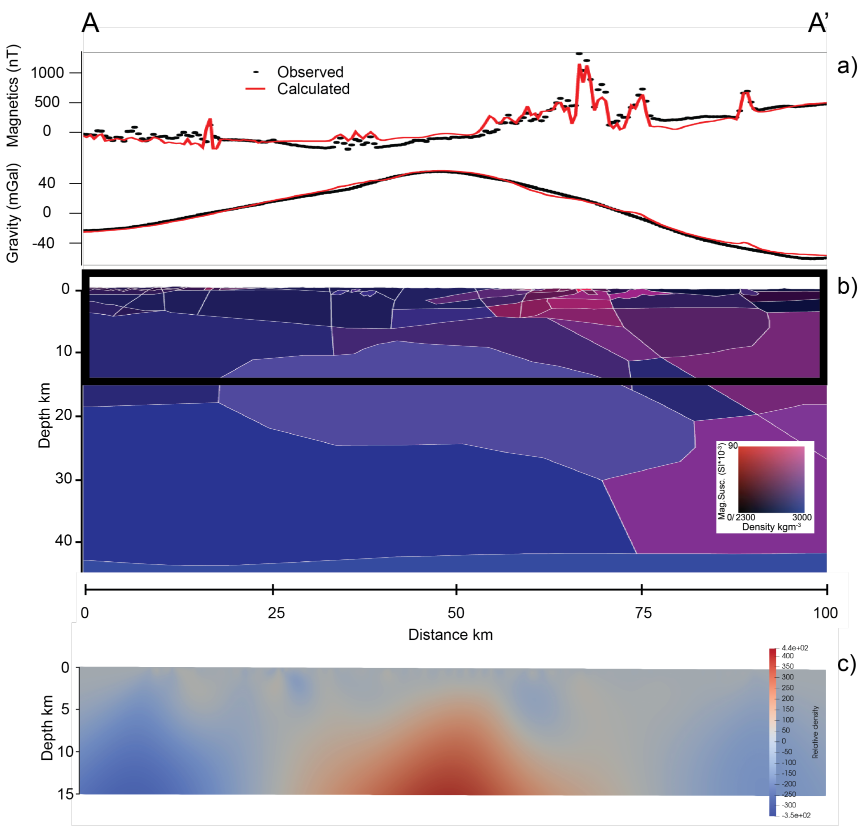

Figure 9. (a) Magnetic and gravity signal (observed) and response calculated from the petrophysical models shown in (b). (b) Combined density and magnetic susceptibility model. The profile is viewed from the southwest, with the location shown in Figure 1. Parts b) and c) adapted from Lindsay et al. (2016).

https://doi.org/10.5194/egusphere-2024-3754
Preprint. Discussion started: 6 January 2025

3.5 Misfit

Examining the spatial relationship between spatial error and misfit can tell us whether spatial error constraints perform a useful role in reducing misfit during inversion. To do this, the spatial distribution of misfit values calculated from the final iteration of inversion is examined. Figure 10 shows the relationship between the magnitude of misfit versus the spatial error. Two models are examined in this figure: (left) inversion using the mean grid and no spatial error constraints and; (right) and inversion using the mean grid and spatial error constraints. We take the absolute misfit values for this representation to focus on magnitude. There is no clear relationship between overall misfit and spatial error when not using spatial error constraints (Figure 10 - left). A noteworthy pattern (or lack of pattern) is seen in the lowest spatial error values. There are many high misfit values in locations close to station locations (i.e. low spatial error values) when not using spatial error. If the inversion was honouring locations with observations, we would expect to see a pattern where low spatial error is associated with low misfit. This is what we see in the plot at right when spatial error is used, especially at locations with spatial error very close to zero. Overall, there is a positive correlation between misfit and spatial error at spatial error values <= 20. The expected pattern is not perfect, and some scatter is present, however a pattern is nonetheless clear. Misfit decreases at spatial error > 20, possibly where the inversion is fitting values with less constraint. It is also worth noting that at spatial error values > 70, misfit values are also high for the inversion using spatial error constraints, while for inversion not using spatial error constraints, these values have a very low misfit, almost certainly being overfit.

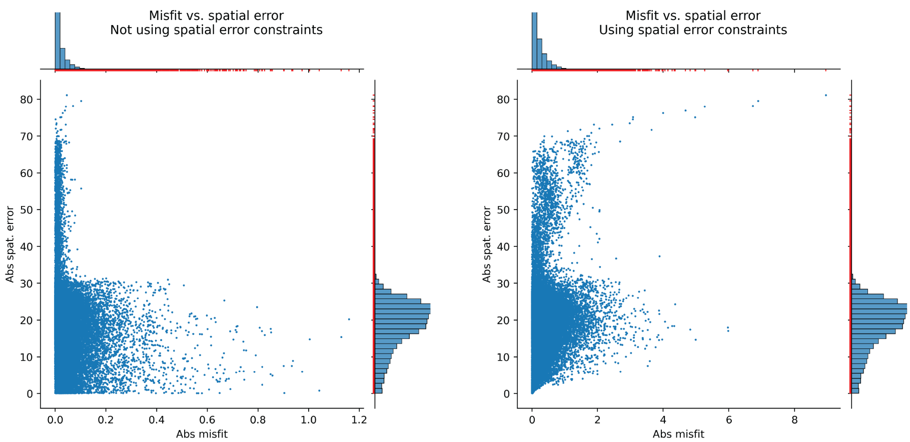

Figure 10. Misfit versus spatial errors are shown with absolute values. Histograms are also shown with red ticks on the axes indicating individual values. Both images show misfit values taken from inversion using the mean model grid input. At left are results obtained when not using spatial error constraints; at right are results when using spatial error constraint. Note the x axis scales differ between images.

The patterns of data cost and spatial error values (Figure 10) demonstrate differences that are interpreted to show a reduction of overfitting. At low values of spatial error (0 < x < 20), low misfit values are also

https://doi.org/10.5194/egusphere-2024-3754
Preprint. Discussion started: 6 January 2025

seen when using spatial error constraints, and locations exhibiting higher spatial error (i.e. further from data points) also exhibit higher misfit. This contrasts with the results from inversion not using spatial error constraints, where there are values of high and low misfit with almost no relationship to spatial error. This is particularly obvious at locations with spatial error <20 and >60.

The positive correlation between misfit and spatial error changes at locations with spatial error 20 < x < 60. Results from inversion using spatial error constraints show a decrease in spatial error 20 < x <30. At misfit > 30, inversion without spatial error constraints shows a sharp decrease in misfit values, as well as reduced variability. At spatial error > 30 for the inversion with spatial error constraints, misfit is reduced, but not to the same degree as without constraints. Overall misfit values increase at spatial error 30 < x < 70, until large misfit values > 2 x > 70.

An analysis of spatial error magnitude is shown in Figure 11. Most spatial error values >30 are located close to the northern boundary. 'Boundary effects' are a well-known phenomena in geospatial studies (Henley, 1981), and are a widely-recognised artefact in geophysical inversion (Zhdanov, 2002). While they can be mitigated or removed (Shapiro, 1970), for the most part they are easily recognised and ignored. Thus the patterns at spatial error values > 30 can safely be ignored.

The most obvious difference between the using and not using spatial error constraints is seen in part c), where the lowest misfit values ≈ 0 are collocated with station locations, and where spatial error is < 10. Part b) does not show any clear spatial relationship between the spatial error and misfit. There are some regions where low misfit values sit in 20 < x < 30 (northwestern quadrant) and the central eastern zone, however these examples are not convincing. Part c) also shows low misfit in the same northwestern quadrant, thus it may be that this region may be simpler to resolve by inversion.

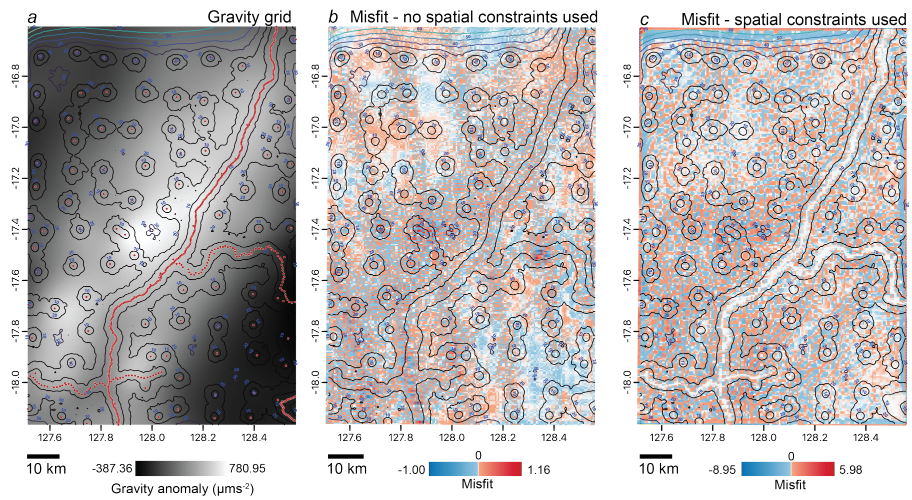

Contours represent spatial error with values as labelled.

Figure 11. Contours of spatial error are plotted against a) the gravity anomaly; b) misfit values from inversion not using spatial error constraints and c) inversion that does use spatial error constraints. Note the dynamic range of misfit values have been scaled to show equivalently high misfit values in b) and c). Station locations are shown in part a) as red points.

https://doi.org/10.5194/egusphere-2024-3754
Preprint. Discussion started: 6 January 2025

At spatial error > 10 the spatial relationship between low misfit looks to become less predictable. This is shown in the more variable misfit values in Figure 10. This is despite the peak we interpret at misfit ≈ 2 and spatial error ≈ 20. Thus, the scatter plot provides an easier interpretation of the utility spatial error constraints provides geophysical inversion for spatial values > 10.

2. Discussion

The combination of the scatter plot and spatial analysis gives confidence that spatial error constraints do guide inversion in a positive fashion. However, there does seem to be a limit at which spatial error constraints are effective. At spatial error > 20, overfitting does seem to occur, and misfit values decrease to those similar to those in the non-spatial error constrained inversion (≈ 0.2). It is not clear why this occurs, however these spatial error values can be used to guide understanding where overfitting may occur prior to the use of inversion in regions of sparse geophysical observations. Overfitting will predominantly occur in the near-surface, so this may be of more interest to people focussed on shallow depths. The spatial error value of 20 may not be generalisable to other regions, however the process outlined here to find the peak in misfit vs spatial error relationship is generalisable to find the threshold of overfitting. Regularisation strength may affect this value, and where higher errors occur, strength can be increased providing additional constraint. The effect of regularisation on what level of spatial error constraint is effective at reducing overfitting has not been explored in this work.

The effects of using spatial error on overfitting have been established by examining the overall data cost and the spatial relationship between misfit and spatial error produced via grid interpolation. The next step is to establish the impact this has on the use of geophysics for mineral exploration. From a practical perspective, one may not care that the inversion has overfitted, especially since visual inversion results are quite similar (Figure 8) and the data cost for the overfitted results are very low. For some, this argument is valid, but it depends on where and what they are interested in.

To better explain, consider a simple example of a mineral explorer using the results of geophysical modelling and interpretation (including inversion, of course) to develop a strategy for deposit discovery. The presence of deeper anomalies can be used for search space reduction and ground selection. The overfitting issue does not impact this activity such that one would change location because overfitting occurred. A deeper anomaly may, for example, change geometry to some degree due to overfitting, but this will unlikely dissuade ground selection at the region or camp-scale. The smaller scale programs following ground selection, such as geochemistry, structural mapping and drilling using the results of geophysical studies can be impacted by inversion overfitting, as near-surface anomalies are typically used to determine survey areas, either as targets or as proxies for some process (e.g. faulting, volcanic activity, or alteration – e.g. Guillen at al. 2008; Lindsay et al. 2020). Remembering that overfitting is essentially trying to fit noise to obtain the lowest misfit (data cost in our case, but can be RMSE, or other metric), small near-surface anomalies are either added or removed to achieve this aim. The result of

https://doi.org/10.5194/egusphere-2024-3754
Preprint. Discussion started: 6 January 2025

adding noise-based anomalies is producing false-positives (Type I error), which add unnecessary expense to smaller-scale activities through unnecessary sampling. Worse is the removal of genuine anomalies and introduction of false-negatives (Type II error), leading to ignored areas and missed opportunities to make a discovery (Neyman & Pearson, 1933).

The consideration of noise, overfitting and Type I and II errors leads to thinking probabilistically. The inversion result using the upper limit gravity dataset (Figure 8) shows smaller, dispersed, strongly negative and shallow-depth anomalies. These anomalies from the upper limit-guided inversion are present in spatial-error constrained and un-constrained inversion. Visual inspection show the position of these anomalies are in locations of spatial error <10, and almost directly under gravity stations (Figure 12). These anomalies could be considered noise, however the assumption that credibility is inversely related to distance from a gravity station would suggest that these anomalies are not.

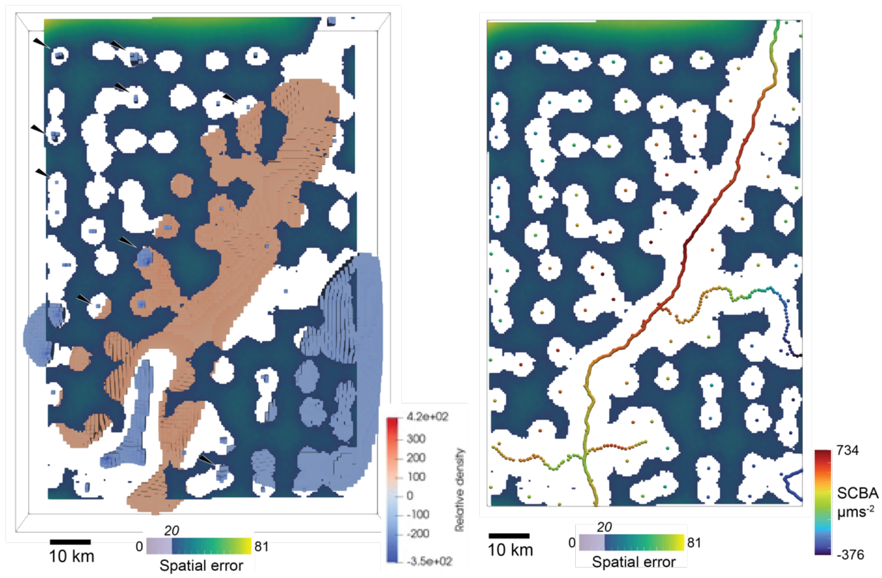

Figure 12. Map view of inversion results using the upper limit gravity grid constrained with spatial error. Spatial error is shown, with the values <20 filtered (note colour scale). At left are the strong negative anomalies with a selection of examples annotated with arrows. (The selection of anomalies is made for visualisation and bears no particular importance). At right are the position of gravity stations and associated measurements for ease of view.

Whether we consider these anomalies credible or not then comes down to how they persist through the full distribution of gravity grid models. The three examples used in this analysis, the mean, lower limit and upper limit are just three slices of an almost infinite number of realisations that can be obtained by sampling different percentiles of the interpolated model. That these small anomalies only feature in one of our three slices would suggest that they are unlikely given they are produced from a gravity realisation that sits in the tails of the probability distribution, but may not be simply noise. Of course, this analysis is underpowered in a statistical sense (i.e. a sample size too small for statistical significance), and a comprehensive analysis would need to consider far more realisations and subject them to inversion. Such probabilistic methods have existed for some years (e.g. Gouveia & Scales, 1998; Sambridge, 1999) and approach this degree of comprehensiveness. Testing the impact of parameters, in our case, three different gravity models, resembles recent work by Martin et al. 2024. They use the Taguchi method to find appropriate petrophysical constraints for geophysical inversion, which requires selection of three levels from the property distribution to emulate a Monte-Carlo sampling process but without the same computational cost (Taguchi, 1987). Indeed, adapting the Taguchi method to the described in this contribution would streamline the process of exploring the geostatistical distribution of geophysical models (including magnetic, seismic and electrical data) used as the observed field for inversion. However, much like these results shown here, accepted solutions tend to revert to the mean when cost functions use metrics that have a Gaussian foundation. In simple terms, even if you do consider the extremes (tails) of the possible realisations, you will likely end up being offered a solution that was obtained by the mean of the geophysical field input for inversion anyway because that solution offers the lowest misfit.

Most inversion schemes will follow a procedure that minimises the misfit to obtain the optimal and thus, most credible solution. Whether the extremes of the data are also investigated and considered is then up to the practitioner. For some, perhaps the status quo is acceptable and due to time and resource pressures, such an investigation is not viable. However, as the analysis presented here suggests that credible results can also be obtained from models constrained by distance from data points and while still exhibiting higher misfits. Importantly, the lowest misfit does not always mean the most credible solution. Spatial error can be obtained from any geostatistical package and does not present a barrier to the practitioner, though finding an inversion package that can use spatial error constraints is harder. The additional time investment in exploring other less likely, but credible solutions, grants the geophysical practitioner a deeper understanding of their data and models, and where and how they may be misrepresenting the properties and structure of the Earth.

Machine learning, including those performing geophysical inversion, is becoming ubiquitous for geoscientific research. Interpolated geophysical grids are commonly used as features in these studies, in particular for mineral potential mapping (e.g. Carranza et al. 2008; Nykänen). The same challenges apply to these types of studies in that the algorithms are unaware of uncertainties related to spatial error. The algorithms, given no other information, assume cell values within a geospatial feature is 'true', and not subject to variability. Some schemes, like Fuzzy Inference Networks (Porwal et al. 2003) can give global confidence weights to a feature, however such weights apply to all cell values. A scheme such using spatial error offers a representative method to convey which locations are supported by observations and give a more thorough evaluation of the features being used in the model.

3. Conclusions

Characterising the Earth's structure is essential for responsible stewardship of natural resources. Much of what we require for metal supply, water and disaster mitigation comes from subsurface imaging facilitated by modelling geophysical data. Time and cost restrictions mean geophysical survey data

https://doi.org/10.5194/egusphere-2024-3754
Preprint. Discussion started: 6 January 2025

acquisition is inconsistent. Some areas are difficult to physically access, while others may not receive attention as they possess lower economic or scientific priority. Regardless of the reason, practitioners are subject to potential errors and unintended effects arising from clustered and sparse geophysical data distributions. Geophysical inversion relies on accurate and representative data. The inversion uses geophysical data as the observed field, representing the 'truth', with a 'misfit' calculated between the proposed or calculated Earth model. The location and magnitude of misfit drive changes to the proposed Earth model and not the geophysical data. Thus, the observed field must be as representative as possible to obtain a representative Earth model. The inversion does not know locations on or near measurement locations and far from measurement locations as the observed field input to inversion is an interpolated grid rather than the geophysical measurements themselves. Geostatistics allows interpolation of property values while providing a spatial error grid describing the errors associated with distance from measurement locations. A spatial error grid calculated using INLA is input to the Tomofast-x geophysical inversion platform with a recently implemented spatial error constraint to represent data distribution for the observed field. The East Kimberley region, northern Western Australia, is a frontier location for critical and base metal exploration and used as a case study using regional gravimetry data. The effect of using spatial error constraints is examined and found to reduce the effects of overfitting, an undesirable effect that is difficult to detect and mitigate. Interpolations selected from the extreme ends of the posterior distribution (the 2.5th and 97.5thpercentiles) are subject to inversion and examined as part of this study to contrast with the usual 'mean' (50th percentile) that is usually the only realisation used in most, non-Bayesian geophysical workflows. Our analysis found inversion results plausible. Reducing the effects of overfitting minimises the chance that near-surface artefacts are produced in the calculated model when the inversion attempts to fit to noise in the observed field. Reducing near-surface artefacts is essential when using models made by inversion for mineral exploration, reducing the number of potentially false targets that need to be investigated or sampled with expensive and time-intensive drilling, ground-sampling and mapping activities. The same approach to spatial error representation applies to machine learning, such as mineral potential modelling or lithological classification, when interpolated grids (geophysical, geochemical or otherwise) are supplied as features. Overfitting is a pervasive issue in geoscience, and the method described here provides a possible solution from commonly available geostatistical methods.

4. Author contributions

ML: Conceptualisation, Data curation, Formal analysis, Investigation, Methodology, Project administration, Visualisation, Writing - original draft preparation/review and editing; VO: Conceptualisation, Formal analysis, Investigation, Methodology, Software, Writing - original draft preparation/review and editing; JG: Conceptualisation, Methodology, Formal analysis, Writing – review and editing, MK: Conceptualisation, Methodology, Writing – review and editing.

5. Competing interests

The authors declare that they have no conflict of interest.

6. Acknowledgments

https://doi.org/10.5194/egusphere-2024-3754
Preprint. Discussion started: 6 January 2025

The authors would like to thank ARC Linkage project 'Loop': Three-dimensional Bayesian Modelling of Geological and Geophysical data (LP210301239), the ARC ITTC 'DARE' (Data Analytics for Resources and Environment) (IC190100031) and MinEx CRC for their support. ML would like to thank Hoël Sielle and Erdinc Saygin (CSIRO) for helpful discussions, sharing ideas and papers on this topic.

This is MinEx CRC Document XX/XX.

7. Data Availability

The data used in this study is found in the CSIRO Data Access Portal (DAP): https://data.csiro.au/collection/csiro:64073

The repository contains the gravity measurements as supplied by Geoscience Australia (Geoscience Australia, 2020), the grids calculated using INLA and the collection of models and misfit calculated using Tomofast-x. File formats are: gravity measurement – shapefile; grids - ERMapper.ers format; 3D inversion models – Visualisation toolkit .vtk format; misfit values – .csv format with x,y,z,*property*.

Tomofast-x is available from GitHub https://github.com/TOMOFAST/Tomofast-x

8. References

Allmendinger, R. W., Siron, C. R., and Scott, C. P.: Structural data collection with mobile devices: Accuracy, redundancy, and best practices, J Struct Geol, 102, 98–112, https://doi.org/https://doi.org/10.1016/j.jsg.2017.07.011, 2017.

Alsi, M., Marcotte, D., and Chouteau, M.: Direct Inversion of Gravity Data by Cokriging, in: Geostat2000, 10, 2000.

Antonio Stamm, F., De La Varga, M., and Wellmann, F.: Actors, actions, and uncertainties: Optimizing decision-making based on 3-D structural geological models, Solid Earth, 10, 2015–2043, https://doi.org/10.5194/se-10-2015-2019, 2019a.

Antonio Stamm, F., De La Varga, M., and Wellmann, F.: Actors, actions, and uncertainties: Optimizing decision-making based on 3-D structural geological models, Solid Earth, 10, 2015–2043, https://doi.org/10.5194/se-10-2015-2019, 2019b.

Aster, R. C., Borchers, B., and Thurber, C. H.: Tikhonov Regularization, in: Parameter Estimation and Inverse Problems, Elsevier, 93–134, https://doi.org/10.1016/B978-0-12-804651-7.00009-2, 2019.

Bodin, T., Sambridge, M., Rawlinson, N., and Arroucau, P.: Transdimensional tomography with unknown data noise, Geophys J Int, 189, 1536–1556, https://doi.org/10.1111/J.1365-246X.2012.05414.X, 2012.

Brisson, S., Wellmann, F., Chudalla, N., von Harten, J., and von Hagke, C.: Estimating uncertainties in 3-D models of complex fold-and-thrust belts: A case study of the Eastern Alps triangle zone,

https://doi.org/10.5194/egusphere-2024-3754
Preprint. Discussion started: 6 January 2025

Applied Computing and Geosciences, 18, 100115, https://doi.org/10.1016/J.ACAGS.2023.100115, 2023.

Carranza, E. J. M., Hale, M., and Faassen, C.: Selection of coherent deposit-type locations and their application in data-driven mineral prospectivity mapping, Ore Geol Rev, 33, 536–558, https://doi.org/10.1016/j.oregeorev.2007.07.001, 2008.

Caumon, G.: Towards stochastic time-varying geological modeling, Math Geosci, 42, 555–569, https://doi.org/10.1007/s11004-010-9280-y, 2010.

Chasseriau, P. and Chouteau, M.: 3D gravity inversion using a model of parameter covariance, J Appl Geophy, 52, 59–74, https://doi.org/10.1016/S0926-9851(02)00240-9, 2003.

Clark, D. A. and Schmidt, P. W.: Petrophysical Properties of the Goonumbla Volcanic Complex, NSW: Implications for Magnetic and Gravity Signatures of Porphyry Cu-Au Mineralisation, Exploration Geophysics, 32, 171–175, 2001.

Cressie, N., Sainsbury-Dale, M., and Zammit-Mangion, A.: Basis-Function Models in Spatial Statistics, Annu Rev Stat Appl, 9, 373–400, https://doi.org/10.1146/annurev-statistics-040120-020733, 2022.

David, M.: Geostatistical Ore Reserve Estimation., Elsevier Science, 27–33 pp., https://doi.org/10.2307/2286639, 2012.

Dentith, M., Enkin, R. J., Morris, W., Adams, C., and Bourne, B.: Petrophysics and mineral exploration: a workflow for data analysis and a new interpretation framework, Geophys Prospect, 68, 178–199, https://doi.org/10.1111/1365-2478.12882, 2020.

Deutch, C. V. and Journel, A. G.: Geostatisical Software Library and User's Guide, Oxford University Press, 1992.

Fairhead, J. D., Cooper, G. R. J., and Sander, S.: Advances in Airborne Gravity and Magnetics, Proceedings of Exploration, 17, 113–127, 2017.

Farquharson, C. G. and Oldenburg, D. W.: Non-linear inversion using general measures of data misfit and model structure, Geophys J Int, 134, 213–227, https://doi.org/10.1046/J.1365-246X.1998.00555.X, 1998.

Gallardo, L. A. and Meju, M. A.: Characterization of heterogeneous near-surface materials by joint 2D inversion of dc resistivity and seismic data, Geophys Res Lett, 30, https://doi.org/10.1029/2003GL017370, 2003.

Gallardo, L. A., Pérez-Flores, M. A., and Gómez-Treviño, E.: Refinement of three-dimensional multilayer models of basins and crustal environments by inversion of gravity and magnetic data, Tectonophysics, 397, 37–54, https://doi.org/10.1016/J.TECTO.2004.10.010, 2005.

Gelman, A., Carlin, J. B., Stern, H. S., Dunson, D. B., Vehtari, A., and Rubin, D. B.: Bayesian Data Analysis, Bayesian Data Analysis, https://doi.org/10.1201/B16018, 2013.

https://doi.org/10.5194/egusphere-2024-3754
Preprint. Discussion started: 6 January 2025

Genichi Taguchi: System of experimental design: engineering methods to optimize quality and minimize costs, UNIPUB/Kraus International Publications, American Supplier Institute, 1987.

Geological Survey of Western Australia: 1:500 000 tectonic units of Western Australia, November 2022 update. Geological Survey of Western Australia, digital data layer, 2022.

Geoscience Australia: Geophysical Acquisition & Processing Section 2020. National Gravity Compilation 2019 (CSCBA), 2020.

Giraud, J., Pakyuz-Charrier, E., Jessell, M., Lindsay, M., Martin, R., and Ogarko, V.: Uncertainty reduction through geologically conditioned petrophysical constraints in joint inversion, Geophysics, 82, ID19–ID34, https://doi.org/10.1190/geo2016-0615.1, 2017.

Giraud, J., Lindsay, M., Ogarko, V., Jessell, M., Martin, R., and Pakyuz-Charrier, E.: Integration of geoscientific uncertainty into geophysical inversion by means of local gradient regularization, Solid Earth, 10, 193–210, https://doi.org/10.5194/se-10-193-2019, 2019a.

Giraud, J., Ogarko, V., Lindsay, M., Pakyuz-Charrier, E., Jessell, M., and Martin, R.: Sensitivity of constrained joint inversions to geological and petrophysical input data uncertainties with posterior geological analysis, Geophys J Int, 218, 666–688, https://doi.org/10.1093/gji/ggz152, 2019b.

Giraud, J., Ogarko, V., Martin, R., Jessell, M., and Lindsay, M.: Structural, petrophysical, and geological constraints in potential field inversion using the Tomofast-x v1.0 open-source code, Geosci. Model Dev, 14, 6681–6709, https://doi.org/10.5194/gmd-14-6681-2021, 2021.

Gouveia, W. P. and Scales, J. A.: Bayesian seismic waveform inversion: Parameter estimation and uncertainty analysis, J Geophys Res Solid Earth, 103, 2759–2779, https://doi.org/10.1029/97JB02933, 1998.

Guillen, A., Calcagno, P., Courrioux, G., Joly, A., and Ledru, P.: Geological modelling from field data and geological knowledge: Part II. Modelling validation using gravity and magnetic data inversion, Physics of the Earth and Planetary Interiors, 171, 158–169, 2008.

Henley, S.: Nonparametric Geostatistics, https://doi.org/10.1007/978-94-009-8117-1, 1981.

Jessell, M., Pakyuz-Charrier, E., Lindsay, M., Giraud, J., and Kemp, E. de: Assessing and Mitigating Uncertainty in Three-Dimensional Geologic Models in Contrasting Geologic Scenarios, Metals, Minerals, and Society, 63–74, https://doi.org/10.5382/SP.21.04, 2018.

Johnson, C. C., Ander, E. L., Lister, T. R., and Flight, D. M. A.: Data conditioning of environmental geochemical data: Quality control procedures used in the British Geological Survey's regional geochemical mapping project, Environmental Geochemistry: Site Characterization, Data Analysis, Case Histories, and Associated Health Issues, 121–147, https://doi.org/10.1016/B978-0-443-13801-0.00001-3, 2024.

Karpatne, A., Ebert-Uphoff, I., Ravela, S., Babaie, H. A., and Kumar, V.: Machine Learning for the Geosciences: Challenges and Opportunities, IEEE Trans Knowl Data Eng, 31, 1544–1554, https://doi.org/10.1109/TKDE.2018.2861006, 2019.

De La Varga, M., Schaaf, A., and Wellmann, F.: GemPy 1.0: Open-source stochastic geological modeling and inversion, Geosci Model Dev, 12, 1–32, https://doi.org/10.5194/gmd-12-1-2019, 2019.

Lane, R. J. L., Wynne, P. E., Djomani, Y. H. P., Stratford, W. R., Barretto, J. A., and Tontini, F. C.: Australian National Gravity Grids Explanatory Notes GEOSCIENCE AUSTRALIA RECORD 2020/22, https://doi.org/10.11636/Record.2020.022, 2019.

Lelièvre, P. G., Oldenburg, D. W., and Williams, N. C.: Integrating geological and geophysical data through advanced constrained inversions*, Exploration Geophysics, 40, 334–341, https://doi.org/doi:10.1071/EG09012, 2009.

Li, Y. and Oldenburg, D. W.: 3-D inversion of magnetic data, Geophysics, 61, 394–408, https://doi.org/10.1190/1.1443968, 1996.

Li, Y. and Oldenburg, D. W.: 3-D inversion of gravity data, Geophysics, 63, 109–119, https://doi.org/10.1190/1.1444302, 1998.

Linde, N., Ginsbourger, D., Irving, J., Nobile, F., and Doucet, A.: On uncertainty quantification in hydrogeology and hydrogeophysics, https://doi.org/10.1016/j.advwatres.2017.10.014, 2017.

Lindsay, M. D., Jessell, M. W., Ailleres, L., Perrouty, S., de Kemp, E., and Betts, P. G.: Geodiversity: Exploration of 3D geological model space, Tectonophysics, 594, 27–37, https://doi.org/10.1016/j.tecto.2013.03.013, 2013.

Lindsay, M. D., Occhipinti, S., Aitken, A. R. A., Metelka, V., Hollis, J., and Tyler, I.: Proterozoic accretionary tectonics in the east Kimberley region, Australia, Precambrian Res, 278, 265–282, https://doi.org/http://dx.doi.org/10.1016/j.precamres.2016.03.019, 2016.

Lindsay, M. D., Occhipinti, S., Laflamme, C., Aitken, A., and Ramos, L.: Mapping undercover : integrated geoscientific interpretation and 3D modelling of a Proterozoic basin, 1053–1077, 2020.

Martin, R., Ogarko, V., Giraud, J., Plazolles, B., Angrand, P., Rousse, S., and Macouin, M.: Gravity data inversion of the pyrenees range using taguchi sensitivity analysis and ADMM bound constraints based on seismic data, Geophys J Int, https://doi.org/10.1093/GJI/GGAE410, 2024.

McGrayne, S. Bertsch.: The theory that would not die : how Bayes' rule cracked the enigma code, hunted down Russian submarines, & emerged triumphant from two centuries of controversy, Yale University Press, 320 pp., 2011.

Moraga, P.: Geospatial Health Data; Modeling and Visualization with R-INLA and Shiny, CRC Press, 1–295 pp., 2020.

Moraga, Paula.: Spatial statistics for data science : theory and practice with R, CRC Press, 279 pp., 2024.

Murray, A. B., Gasparini, N. M., Goldstein, E. B., and van der Wegen, M.: Uncertainty quantification in modeling earth surface processes: More applicable for some types of models than for others, Comput Geosci, 90, 6–16, https://doi.org/10.1016/j.cageo.2016.02.008, 2016.

https://doi.org/10.5194/egusphere-2024-3754
Preprint. Discussion started: 6 January 2025

Neyman, J. and Pearson, E. S.: IX. On the problem of the most efficient tests of statistical hypotheses, Philosophical Transactions of the Royal Society of London. Series A, Containing Papers of a Mathematical or Physical Character, 231, 289–337, https://doi.org/10.1098/RSTA.1933.0009, 1933.

Nykänen, V.: Radial basis functional link nets used as a prospectivity mapping tool for orogenic gold deposits within the central lapland greenstone belt, Northern Fennoscandian shield, Natural Resources Research, 17, 29–48, https://doi.org/10.1007/s11053-008-9062-0, 2008.

Ogarko, V., Giraud, J., Martin, R., and Jessell, M.: Disjoint interval bound constraints using the alternating direction method of multipliers for geologically constrained inversion: Application to gravity data, Geophysics, 86, G1–G11, https://doi.org/10.1190/GEO2019-0633.1, 2021a.

Ogarko, V., Frankcombe, K., Liu, T., Giraud, J., Martin, R., and Jessell, M.: Tomofast-x 2.0: an open-source parallel code for inversion of potential field data with topography using wavelet compression, Geosci. Model Dev, 17, https://doi.org/10.5194/gmd-17-2325-2024, 2021b.

Olierook, H. K. H., Scalzo, R., Kohn, D., Chandra, R., Farahbakhsh, E., Clark, C., Reddy, S. M., and Müller, R. D.: Bayesian geological and geophysical data fusion for the construction and uncertainty quantification of 3D geological models, https://doi.org/10.1016/j.gsf.2020.04.015, 2020.

Paige, C. C. and Saunders, M. A.: LSQR: An Algorithm for Sparse Linear Equations and Sparse Least Squares, ACM Transactions on Mathematical Software (TOMS), 8, 43–71, https://doi.org/10.1145/355984.355989/ASSET/CF3C8EE0-D698-4E67-BD8A-BF0B25681EEC/ASSETS/355984.355989.FP.PNG, 1982.

Pakyuz-Charrier, E., Giraud, J., Ogarko, V., Lindsay, M., and Jessell, M.: Drillhole uncertainty propagation for three-dimensional geological modeling using Monte Carlo, Tectonophysics, 747–748, 16–39, https://doi.org/https://doi.org/10.1016/j.tecto.2018.09.005, 2018a.

Pakyuz-Charrier, E., Lindsay, M., Ogarko, V., Giraud, J., and Jessell, M.: Monte Carlo simulation for uncertainty estimation on structural data in implicit 3-D geological modeling, a guide for disturbance distribution selection and parameterization, Solid Earth, 9, 385–402, https://doi.org/10.5194/se-9-385-2018, 2018b.

Pirot, G., Krityakierne, T., Ginsbourger, D., and Renard, P.: Contaminant source localization via Bayesian global optimization, Hydrol Earth Syst Sci, 23, 351–369, https://doi.org/10.5194/hess-23-351-2019, 2019.

Porwal, A., Carranza, E. J. M., and Hale, M.: Knowledge-Driven and Data-Driven Fuzzy Models for Predictive Mineral Potential Mapping, Natural Resources Research, 12, 1–25, 2003.

Posit team: RStudio: Integrated Development Environment for R, http://www.posit.co/, 2023.

Quigley, M. C., Bennetts, L. G., Durance, P., Kuhnert, P. M., Lindsay, M. D., Pembleton, K. G., Roberts, M. E., and White, C. J.: The provision and utility of earth science to decision-makers:

https://doi.org/10.5194/egusphere-2024-3754
Preprint. Discussion started: 6 January 2025

synthesis and key findings, Environ Syst Decis, 39, 349–367, https://doi.org/10.1007/s10669-019-09737-z, 2019a.

Quigley, M. C., Bennetts, L. G., Durance, P., Kuhnert, P. M., Lindsay, M. D., Pembleton, K. G., Roberts, M. E., and White, C. J.: The provision and utility of science and uncertainty to decision-makers: earth science case studies, Springer US, 307–348 pp., https://doi.org/10.1007/s10669-019-09728-0, 2019b.

R Core Team: R: A Language and Environment for Statistical Computing, https://www.r-project.org/, 2023.

Rashidifard, M., Giraud, J., Lindsay, M., Jessell, M., and Ogarko, V.: Constraining 3D geometric gravity inversion with a 2D reflection seismic profile using a generalized level set approach: application to the eastern Yilgarn Craton, Solid Earth, 12, 2387–2406, https://doi.org/10.5194/SE-12-2387-2021, 2021.

Reid, A. B. and Thurston, J. B.: The structural index in gravity and magnetic interpretation: Errors, uses, and abuses, Geophysics, 79, J61–J66, https://doi.org/10.1190/geo2013-0235.1, 2014.

Rue, H., Martino, S., and Chopin, N.: Approximate Bayesian Inference for Latent Gaussian models by using Integrated Nested Laplace Approximations, J R Stat Soc Series B Stat Methodol, 71, 319–392, https://doi.org/10.1111/J.1467-9868.2008.00700.X, 2009.

Sainsbury-Dale, M., Zammit-Mangion, A., and Cressie, N.: Modeling Big, Heterogeneous, Non-Gaussian Spatial and Spatio-Temporal Data Using FRK, J Stat Softw, 108, 1–39, https://doi.org/10.18637/JSS.V108.I10, 2024.

Sambridge, M.: Geophysical inversion with a neighborhood algorithm - II. Appraising the ensemble, Geophys, J. Int., 138, 727–746, 1999.

Sambridge, M., Bodin, T., Gallagher, K., and Tkalcic, H.: Transdimensional inference in the geosciences, Philosophical Transactions of the Royal Society A: Mathematical, Physical and Engineering Sciences, 371, https://doi.org/10.1098/RSTA.2011.0547, 2013.

Scales, J. A. and Snieder, R.: To Bayes or not to Bayes?, Geophysics, 62, 1045–1046, https://doi.org/10.1190/1.6241045.1, 1997.

Scales, J. A. and Snieder, R.: What is noise?, GEOPHYSICS, 63, https://doi.org/https://doi.org/10.1190/1.1444411, 1998.

Seillé, H., Visser, G., Markov, J., and Simpson, J.: Probabilistic Cover-Basement Interface Map in Cloncurry, Australia, Using Magnetotelluric Soundings, J Geophys Res Solid Earth, 126, e2021JB021883, https://doi.org/10.1029/2021JB021883, 2021.

Sivarajah, Y., Holden, E., Togneri, R., Dentith, M., and Lindsay, M.: Visual saliency and potential field data enhancements: Where is your attention drawn?, Interpretation, 2, T155–T167, https://doi.org/doi:10.1190/INT-2013-0199.1, 2014.

Stoch, B., Basson, I. J., Gloyn-Jones, J. N., and Lomberg, K. G.: The influence of variable anisotropic search parameters on implicitly-modelled volumes and estimated contained metal in a structurally-complex gold deposit, Ore Geol Rev, 142, 104719, https://doi.org/10.1016/J.OREGEOREV.2022.104719, 2022.

Swain, C. J.: A FORTRAN IV program for interpolating irregularly spaced data using the difference equations for minimum curvature, Comput Geosci, 1, 231–240, 1976.

Tarantola, A.: Inverse problem theory and methods for model parameter estimation, Society for Industrial and Applied Mathematics, 2005.

Tarantola, A.: Popper, Bayes and the inverse problem, Nat Phys, 2, 492–494, 2006.

Tikhonov, A. N. and Arsenin, V. Y.: Solutions of ill-posed problems, 1977.

Torvela, T. and Bond, C. E.: Do experts use idealised structural models? Insights from a deepwater fold-thrust belt, J Struct Geol, 33, 51–58, https://doi.org/10.1016/j.jsg.2010.10.002, 2011.

Tyler, I. M. and Phillips, C.: Sally Downs Supersuite (P_-SD-xg-o), Perth, 2021.

Wang, J. and Zuo, R.: Spatial modelling of hydrothermal mineralization-related geochemical patterns using INLA+SPDE and local singularity analysis, Comput Geosci, 154, 104822, https://doi.org/10.1016/J.CAGEO.2021.104822, 2021.

Wellmann, F. and Caumon, G.: 3-D Structural geological models: Concepts, methods, and uncertainties, Advances in Geophysics, 59, 1–121, https://doi.org/10.1016/bs.agph.2018.09.001, 2018.

Wellmann, J. F. and Regenauer-Lieb, K.: Uncertainties have a meaning: Information entropy as a quality measure for 3-D geological models, Tectonophysics, https://doi.org/doi:10.1016/j.tecto.2011.05.001, 2011.

Wilson, C. G., Bond, C. E., and Shipley, T. F.: How can geologic decision-making under uncertainty be improved?, Solid Earth, 10, 1469–1488, https://doi.org/10.5194/se-10-1469-2019, 2019.

Zhdanov, M. S.: Geophysical inverse theory and regularization problems, Elsevier, 2002.